

Original research article

Theoretical analysis of highly temperature-sensitive fem based optical sensor in the infrared range



Hasan Abdullah^a, Md. Rafiqul Islam^a, Kawsar Ahmed^{a,b}, Dror Malka^d, Truong Khang Nguyen^{e,f}, Md. Nadim Hossain^a, Bikash Kumar Paul^{a,b,c}, Vigneswaran Dhasarathan^{e,f,*}

^a Department of Information and Communication Technology, Mawlana Bhashani Science and Technology University, Santosh, Tangail, 1902, Bangladesh

^b Group of Bio-photomatrix, Mawlana Bhashani Science and Technology University, Santosh, Tangail, 1902, Bangladesh

^c Department of Software Engineering, Daffodil International University, Sukrabad, Dharmamondi, Dhaka, 1207, Bangladesh

^d Faculty of Engineering, Holon Institute of Technology (HIT), Holon, 5810201, Israel

^e Division of Computational Physics, Institute for Computational Science, Ton Duc Thang University, Ho Chi Minh City, Vietnam

^f Faculty of Electrical and Electronics Engineering, Ton Duc Thang University, Ho Chi Minh City, Vietnam

ARTICLE INFO

Keywords:

Tempearture sensor
Photonic crystal fiber (PCF)
Refractive index
FEM

ABSTRACT

This paper demonstrates a highly sensitive temperature sensor based on photonic crystal fiber (PCF) to evaluate the temperature of an analyte. The proposed structure is evaluated by a finite-element method (FEM) which is composed of one silica core and an analyte core. The maximum wavelength sensitivity of 29,411.765 nm/refractive-index unit (RIU) and the maximum temperature sensitivity of 5000 pm/°C are recorded for the proposed PCF based temperature sensor. According to our knowledge, this measurement represents the maximum sensitivity response to the PCF based temperature sensor. Additionally, the temperature is tuned between 30–60 °C for getting highest sensitivity response. Besides, the peak wavelength shifts, different loss spectra are also investigated for the proposed model. In the future, this proposed structure can be used for multiple sensing purposes such as gas sensing, biomedical sensing, salinity sensing, chemical sensing with modification and analyzing upon this structure.

1. Introduction

PCF is one of the greatest platforms for sensing technology because of its intrinsic design versatility [1]. The uses of temperature sensor have been increased rapidly in recent years. Temperature sensing technology with special structure and simple remote control plays a vital role in various applications such as transport, industrial, entertainment uses and health. Temperature sensor based on PCF has a greater impact for its magnificent optical performance. Nowadays PCF is being used for various application for example temperature sensing [2,3], gas sensing [4], pH sensing [5], dew sensing [6], chemical sensing [7], magnetic sensing [8,9], salinity sensing [10], strain sensing [11,12], current sensing [13], pressure sensing [14,15], viscosity sensing [16], humidity sensing [17,18] etc. For increasing sensing applications, various shaped sensors have been promoted such as U-shaped-fiber [19], D-shaped-fiber [20], two Peanut-shaped-fiber [21], tapered-fiber [22], etc. Many sensing techniques can be applied in the significant area of

* Corresponding author at: Division of Computational Physics, Institute for Computational Science, Ton Duc Thang University, Ho Chi Minh City, Vietnam.

E-mail address: vigneswaran.d@tdtu.edu.vn (V. Dhasarathan).

temperature detection, salinity-detection, glucose detection, antibody detection and biochemical [23–27].

In 2008, Chen et al. [28] demonstrated a fiber-Bragg-grating sensor which showed a sensitivity of 10.47 pm/°C and the evaluated temperature range was 0 – 140 °C. Although, investigated temperature range was high but the sensitivity response was not very much high. In the same year, Pang et al. [29] reported a PCF based temperature sensor which showed a sensitivity of 240 pm/°C, where temperature varied from -20 °C to 80 °C. This result shows a slight high sensitivity but this is not good enough. After that, Peng et al. [30] designed surface plasmon resonance (SPR) based temperature sensor which provided a sensitivity of 720 pm/°C and the range of temperature was 0 – 100 °C. The authors improved the sensitivity compared to the previously reported articles. But, the authors used the gold layer in their structure which increased the fabrication cost. In 2014, Wu et al. [31] reported an optical fiber based temperature sensor which showed a sensitivity of 0.8833 nm/°C and 0.7896 nm/°C, where temperature detecting windows were 10 °C and 20 °C respectively. The authors improved the sensitivity but the investigated temperature range was very small. In the meantime, Zhao et al. [32] and Zhen et al. [33] showed temperature sensor based on an optical fiber Sagnac interferometer (OFSI) that obtained the sensitivity of -0.4 nm/°C and -1.17 nm/°C respectively. The authors used selectively liquid as an analyte in their proposed structure and improved the sensitivity response respectively. In 2018, Vigneswaran et al. [34] were proposed PCF based salinity sensor where seawater was used as an analyte. They have investigated only wavelength based sensing of seawater but not temperature based sensing properties. After that in the earlier year of 2019, Alam et al. [35] reported dual core temperature sensor based on PCF where water was used an analyte. Besides, they have investigated both wavelength based sensing and temperature based sensing properties. They have gained the sensitivity of 25,000 nm/RIU and 818 pm/°C respectively. Although, the authors improved the wavelength sensitivity response, the temperature sensitivity was not in standard level. From the literature review, it can be concluded that there is still room to design PCF based temperature sensor to gain more wavelength sensitivity response as well as temperature sensitivity response.

In this paper, we have designed a temperature sensor based on silica core mode. Besides, seawater is injected in the analyte core following article [34] and fused silica is used as background material. The investigation is evaluated by the finite-element method (FEM). The observed temperature sensitivity and wavelength sensitivity is better than the above-reported articles.

2. Structure design

The cross-section of the reported temperature sensor based on PCF is shown in Figs. 1 and 2. The polygonal air holes are represented in a hexagonal pattern with the lattice pitch $P_1 = P_2 = 2.6 \mu\text{m}$. The central hole is removed and it performs as silica core. Fig. 1 shows diagonal lengths of all air holes including analyte core where $d_1 = 1.6 \mu\text{m}$ and $d_2 = 2.4 \mu\text{m}$ for hexagonal PCF-1 structure. Similarly Fig. 2 shows diagonal lengths of all air holes including analyte core where $d_3 = 1.4 \mu\text{m}$ and $d_4 = 2.2 \mu\text{m}$ for hexagonal PCF-2 structure. The analyte core is represented with blue color which is situated directly right to the silica core. For the inner cladding layer, the diameter is 21.2 μm and for outer, it is 23.2 μm. The refractive index of fused silica which is used as background material is calculated using Sellmeier equation [36]:

$$n^2(\lambda, T) = (1.31552 + 6.90754 \times 10^{-6}T) + \frac{(0.788404 + 23.5835 \times 10^{-6}T)\lambda^2}{\lambda^2 - (0.0110199 + 0.584758 \times 10^{-6}T)} + \frac{(0.91316 + 0.548368 \times 10^{-6}T)\lambda^2}{\lambda^2 - 100} \quad (1)$$

where n is effective RI, λ represents wavelength in μm and T represents temperature in °C. The RI of seawater is determined by the following equation [34]:

$$n(S_l, \lambda_p, T) = 1.3104 + (1.779 \times 10^{-4} - 1.05 \times 10^{-6}T)S_l + (1.6 \times 10^{-8}T^2)S_l - \frac{4382}{\lambda^2} - 2.02 \times 10^{-6} \times T^2 \\ + \frac{15.868 + 0.01155S_l - 0.00423T}{\lambda} + \frac{1.1455 \times 10^{-6}}{\lambda^3} \quad (2)$$

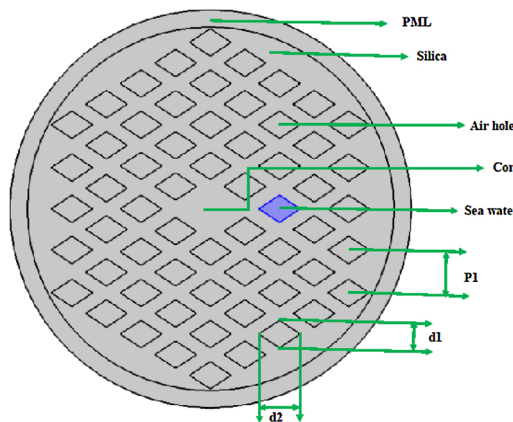


Fig. 1. Cross-sectional view of the proposed hexagonal PCF-1 structure.

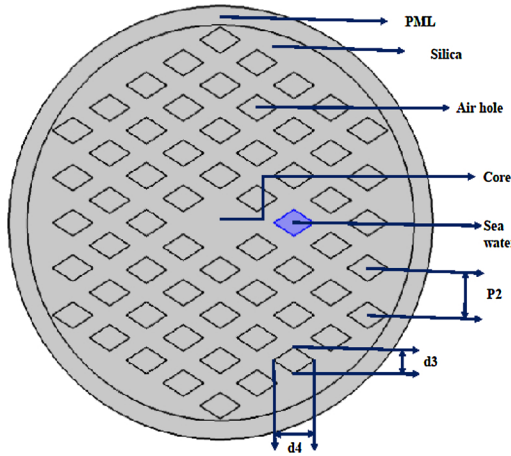


Fig. 2. Cross-sectional view of the proposed hexagonal PCF-2 structure.

Where n is RI of sea water in RIU, salinity of water is S_i , λ represents wavelength in μm and T represents temperature in $^{\circ}\text{C}$.

3. Results Analysis and Discussion

In this section, the outcomes of the proposed models are analyzed and discuss briefly in subsection 3.1 to 3.7 respectively.

3.1. Mode analysis and Refractive Index

Core mode is considered for the desired result analysis. Core mode has two polarizations, one is X polarization and another is Y polarization. Fig. 3(a) and (b) shows the silica core mode for X and Y polarization respectively for hexagonal PCF-1 structure. Similarly, Fig. 3(c) and (d) shows the silica core mode for X and Y polarization respectively for hexagonal PCF-2 structure. Fig. 4 represents the relationship between refractive index and wavelength. From this figure, it is observable that refractive index is inversely proportional to the wavelength.

3.2. Confinement Loss Calculations

The confinement loss is a very significant parameter for PCF based temperature sensor. It is calculated using the following Eq. (3) [34,37]

$$\propto(x, y) = 8.686 \times \frac{2\pi}{\lambda} \times \text{Im}[n_{\text{eff}}] \times 10^6 \quad (3)$$

Where, confinement loss (\propto) is in dB/m and wavelength (λ) is in micrometer unit. $\text{Im}[n_{\text{eff}}]$ is the imaginary part of effective RI. Fig. 5(a) and (b) shows the confinement loss of core mode in X polarization and Y polarization-mode for hexagonal PCF-1 structure. Similarly, Fig. 6(a) and (b) shows the confinement loss of core mode in X polarization and Y polarization mode field distribution for hexagonal PCF-2 structure. Combination of confinement loss spectra is shown in Fig. 7 for X polarization and Y polarization for both structures. The operating wavelength range is 1600 nm–1700 nm and temperature range is 30–60 $^{\circ}\text{C}$ for both PCF structure. For hexagonal PCF-1 structure, the peak loss varies from 2E-09 to 5.5E-09 dB/m where maximum loss is attained 5.5E-09 dB/m for 40 $^{\circ}\text{C}$ at the wavelength 1680 nm for the X polarization. For Y polarization, the peak loss varies from 1.9E-09 to 4.5E-09 dB/m where maximum loss is attained 4.5E-09 dB/m for 50 $^{\circ}\text{C}$ at the wavelength 1630 nm. In hexagonal PCF-2 structure, the peak loss varies from 4.3E-09 to 7.5E-09 dB/m where maximum loss is attained 7.5E-09 dB/m for 50 $^{\circ}\text{C}$ at the wavelength 1640 nm for the X polarization. For Y polarization, the peak loss varies from 2.1E-09 to 4.3E-09 decibel per meter where utmost loss is attained 4.3E-09 dB/m for 60 $^{\circ}\text{C}$ at the wavelength 1610 nm.

3.3. Peak wavelength versus temperature

Figs. 5 and 6 displays that peak wavelength is increasing with the decrease in temperature. This relationship is shown in Fig. 8(a) and (b) where peak spectra is maximum at temperature 30 $^{\circ}\text{C}$. The topmost wavelength is more decreasing for X polarization than Y

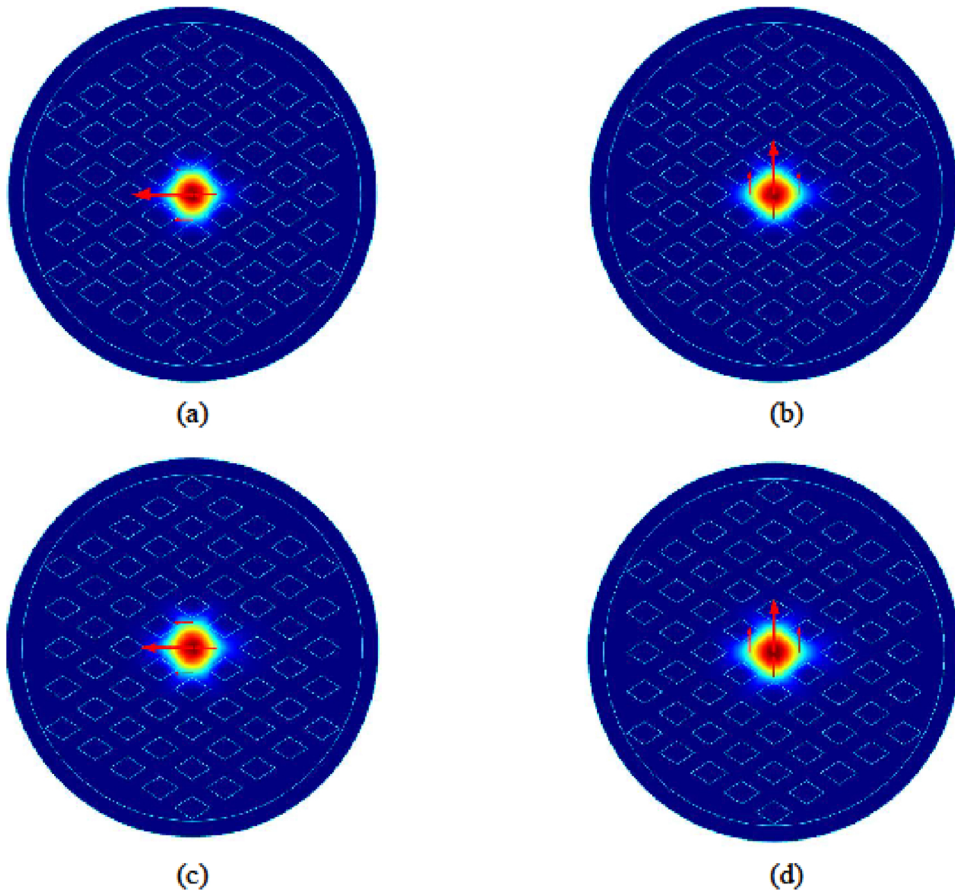


Fig. 3. Mode propagation of (a) silica core mode for X polarization (b) silica core mode for Y polarization for hexagonal PCF-1 structure and (c) silica core mode for X polarization (d) silica core mode for Y polarization for hexagonal PCF-2 structure.

polarization after 50 °C in Fig. 8(a). In Fig. 8(b), the peak wavelength is also decreased with increasing temperature but the wavelength is more decreasing for 40–50 °C.

3.4. Wavelength shift versus temperature

Wavelength shift is the difference between two topmost wavelengths of adjacent temperature. Working temperature is changed from 30–60 °C so the wavelength shift will be 40–60 °C. In Fig. 9, the wavelength shift is displayed with respect to the temperature. It is clear that the wavelength shift is increased when the temperature is increased.

3.5. Sensitivity measurement

Sensitivity is measured using the following equation [38]:

$$S = \frac{\Delta\lambda_{peak}}{\Delta n} \quad (4)$$

where, Δn is RI difference and $\Delta\lambda_{peak}$ is peak wavelength difference. Above formula shows that sensitivity is proportional to the $\Delta\lambda_{peak}$. Maximum peak wavelength difference is required for high sensitivity. Hexagonal PCF-1 structure provides better sensitivity. So, all the below sensitivity measurements are only for hexagonal PCF-1 structure. Fig. 10(a) and (b) shows the sensitivity curve for X polarization. From the curve, it is clear that sensitivity is increasing with the decreasing in temperature. From Fig. 10 it is observable that peak wavelength is the highest when the temperature changes from 30 °C to 40 °C. The highest wavelength sensitivity response is 29411.765 nm/RIU at 40 °C for X polarization in Table 1. Table 2 displays temperature sensitivity calculations for X polarization and the maximum temperature sensitivity is 5000 (pm/°C) at temperature 40 °C. For Y polarization, the highest wavelength sensitivity

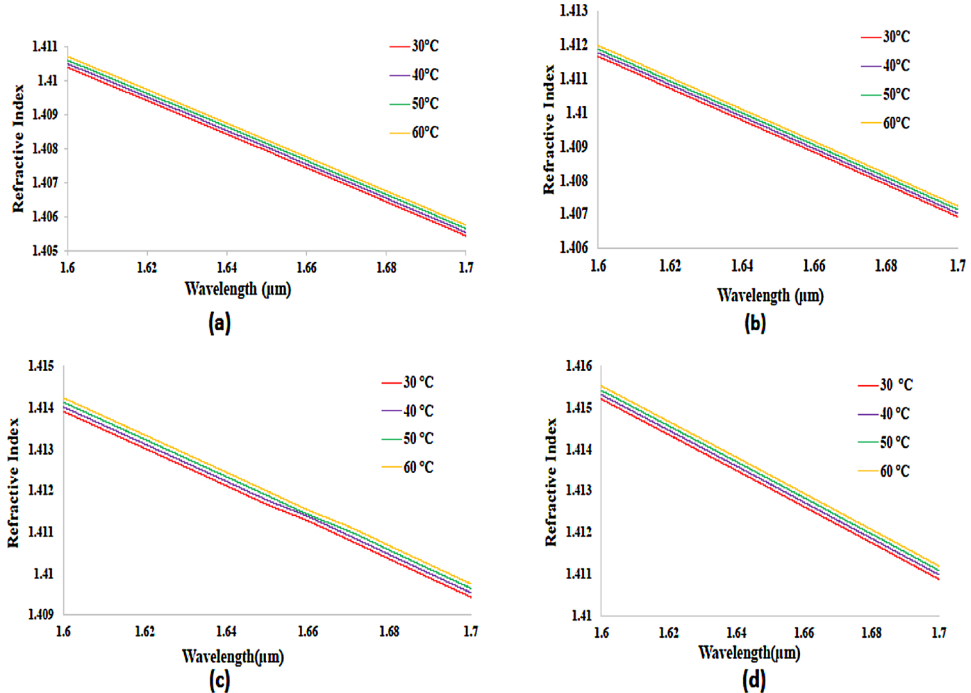


Fig. 4. Refractive Index of (a) X polarization and (b) Y polarization for PCF-1 structure and (c) X polarization (d) Y polarization for PCF-2 structure.

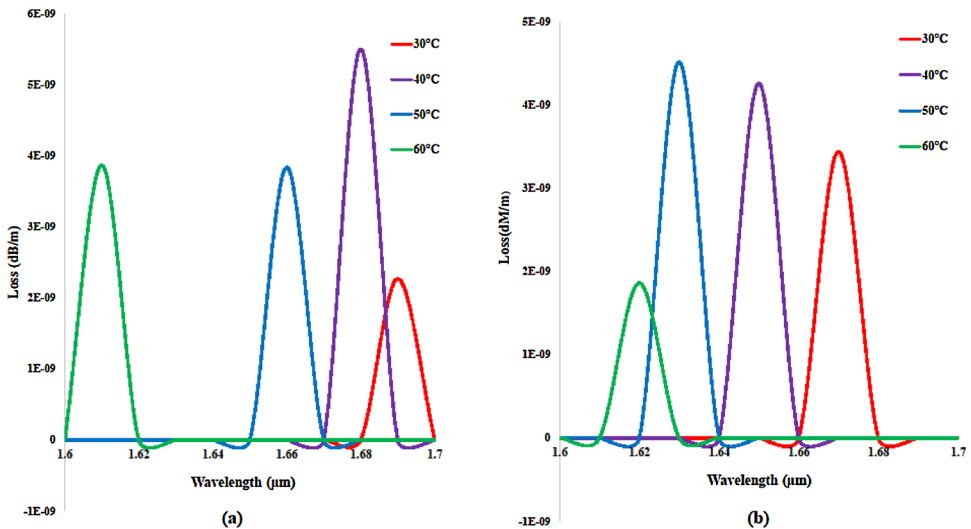


Fig. 5. Confinement loss spectra of (a) X polarization (b) Y polarization for hexagonal PCF-1 structure.

response is 15384.62 nm/RIU at 40 °C in Table 3. Table 4 shows the temperature sensitivity response for Y polarization where the maximum temperature sensitivity response is 5000 (pm/°C) at 40 °C and 50 °C.

3.6. Effect of diagonal on sensitivity

Structural design is very much significant because temperature sensing result depends on it. If the diagonal of air holes or core varies then the result can be changed. In this work, two different diagonals are used for air holes including the core. Diagonals $d_1 =$

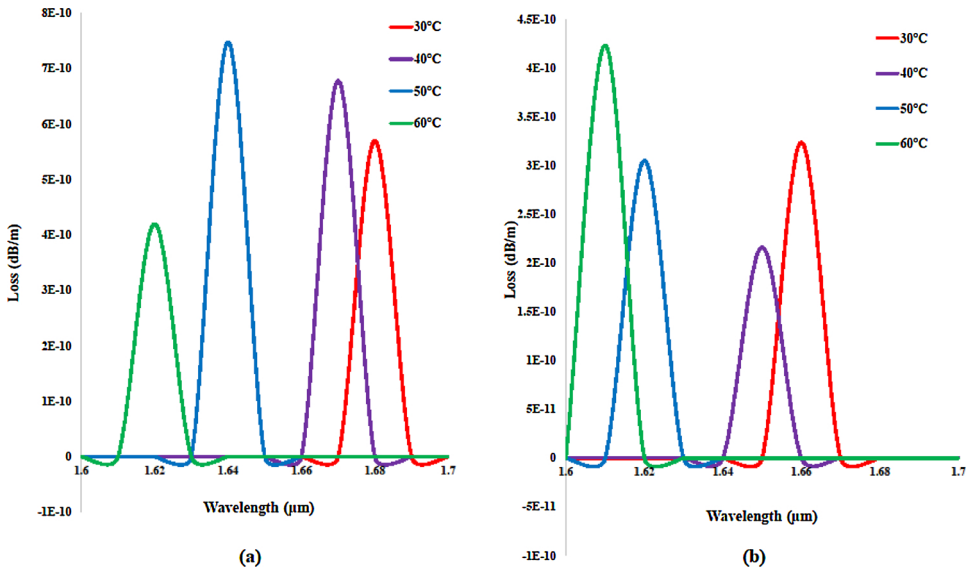


Fig. 6. Confinement loss spectra of (a) X polarization (b) Y polarization for hexagonal PCF-2 structure.

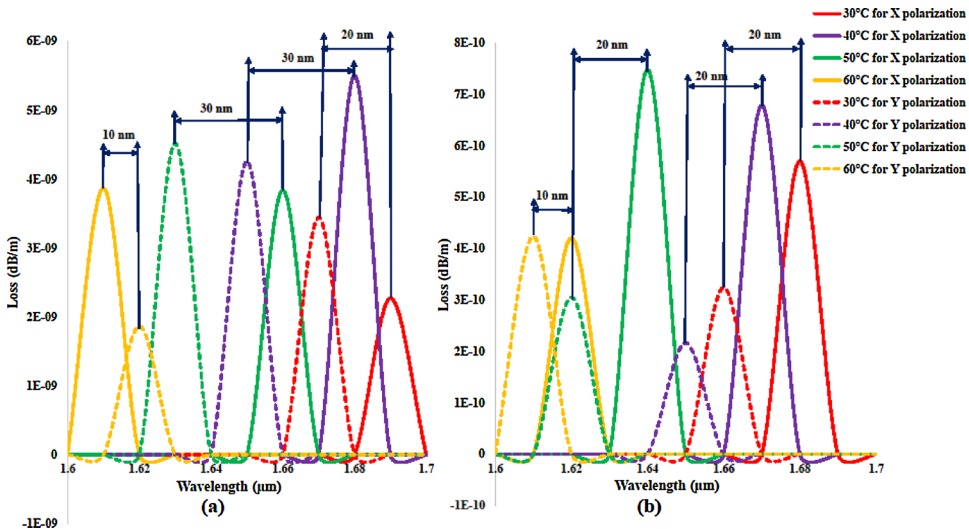


Fig. 7. Confinement loss spectra with wavelength deviation for (a) PCF-1 and (b) PCF-2.

$1.6 \mu\text{m}$ and $d_2 = 2.4 \mu\text{m}$ are used in hexagonal PCF-1 structure and diagonals $d_3 = 1.4 \mu\text{m}$ and $d_4 = 2.2 \mu\text{m}$ are used in hexagonal PCF-2 structure for all the air holes and core. The standard values of diagonals are $d_1 = 1.6 \mu\text{m}$ and $d_2 = 2.4 \mu\text{m}$ as it provides better sensitivity.

3.7. Sensitivity Comparison

Table 5 shows the comparison of wavelength sensitivity performance and temperature sensitivity performance between previously published articles and this proposed article. It is clear that this proposed sensor has obtained the highest wavelength sensitivity performance and temperature sensitivity performance compare to the previously published articles.

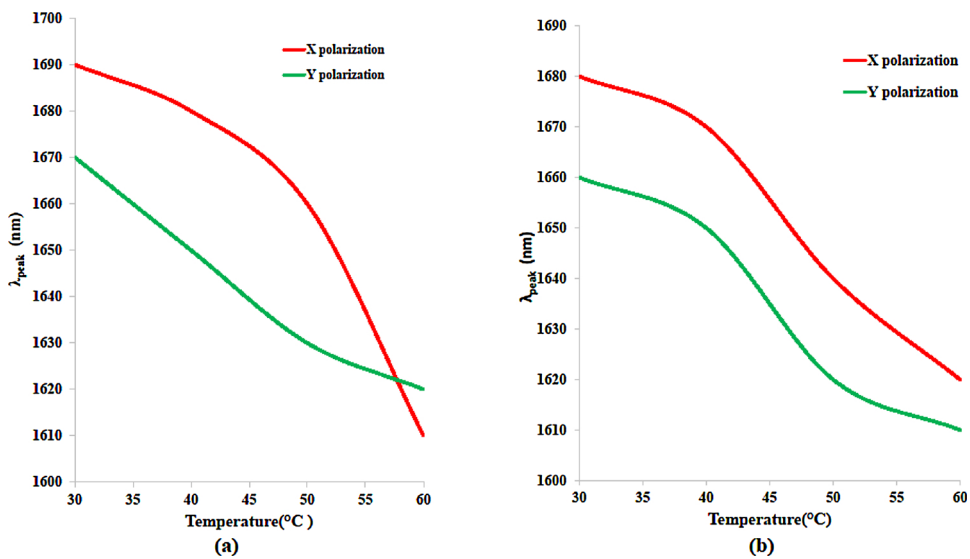


Fig. 8. Peak wavelength spectra for 30 – 60 °C temperature of (a) hexagonal PCF-1 structure and (b) hexagonal PCF-2 structure.

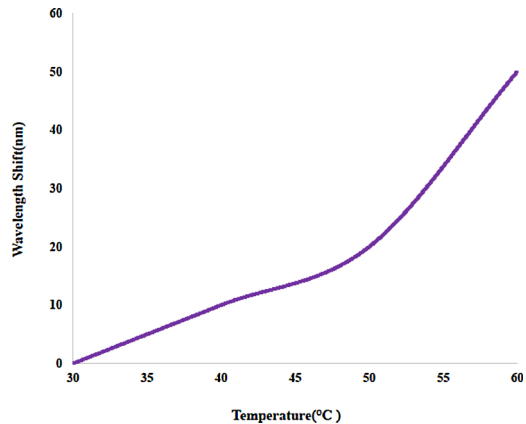


Fig. 9. Wavelength shift spectra of X polarization for PCF-1 structure.

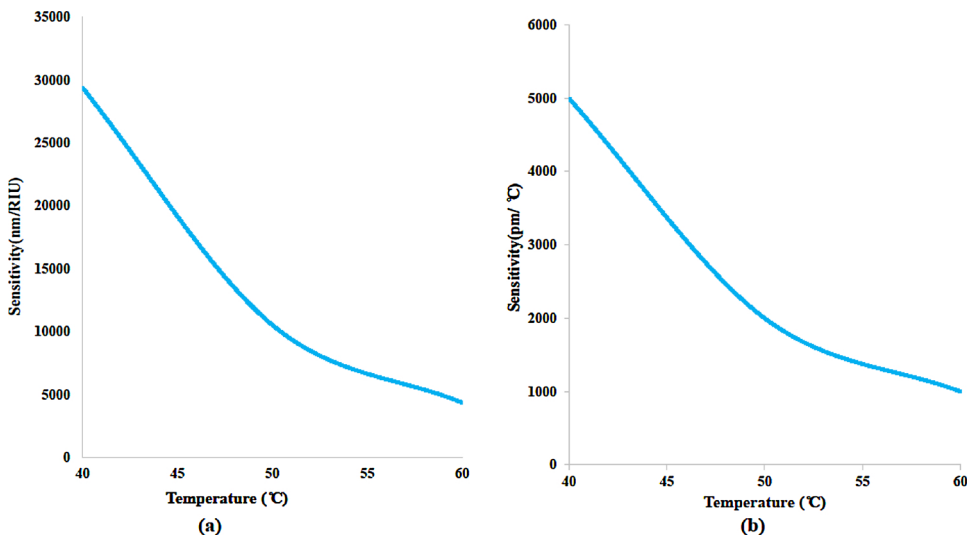


Fig. 10. (a) Wavelength sensitivity (b) Temperature sensitivity for X polarization.

Table 1

Wavelength sensitivity measurement table of X polarization.

Temperature (°C)	Peak Wavelength(μm)	RIU	Δλ(nm)	Δn	Δλ/Δn(nm)
30	1.61	1.3203			
40	1.66	1.3186	50	.0017	29411.765
50	1.68	1.3167	20	.0019	10526.31
60	1.69	1.3144	10	.0023	4347.83

Table 2

Temperature sensitivity measurement table of X polarization.

Temperature (°C)	Peak Wavelength(μm)	Δλ(pm)	ΔT(°C)	Δλ/ΔT (pm/°C)
30	1.61			
40	1.66	50000	10	5000
50	1.68	20000	10	2000
60	1.69	10000	10	1000

Table 3

Wavelength sensitivity measurement table of Y polarization.

Temperature (°C)	Peak Wavelength(μm)	RIU	Δλ(nm)	Δn	Δλ/ΔT (pm/°C)
30	1.67	1.3200			
40	1.65	1.3187	20	.0013	15384.62
50	1.63	1.3169	20	.0018	11111.11
60	1.62	1.3147	10	.0022	4545.45

Table 4

Temperature sensitivity measurement table of Y polarization.

Temperature (°C)	Peak Wavelength(μm)	Δλ(pm)	ΔT(°C)	Δλ/ΔT (pm/°C)
30	1.67			
40	1.65	20000	10	2000
50	1.63	20000	10	2000
60	1.62	10000	10	1000

Table 5

Comparison of wavelength sensitivity performance and temperature sensitivity performance among previously published articles.

Structures	Wavelength Sensitivity(nm/RIU)	Temperature Sensitivity(pm/°C)	Ref.
Fiber-Bragg-grating sensor	-	10.47	[28]
PCF based Temperature Sensor	-	240	[29]
SPR based Temperature Sensor	-	720	[30]
PCF based Salinity Sensor	5675	-	[34]
Temperature Sensor using dual-core PCF	25000	818	[35]
Temperature Sensor using hexagonal PCF	29411.765	5000	This work

4. Conclusion

In this article, a highly sensitive temperature sensor based on PCF has been recommended using FEM. Design and implementation of this proposed sensor have been done using COMSOL Multiphysics version 5.3a. which is a popular software package based on FEM. A temperature-sensitive component is injected in a hole that is situated horizontally with the central silica core and it works as an analyte. Moreover, the middle of the proposed PCF is a defect silica core. Complete statistical analysis has been conceded for the temperature ranging from 30–60 °C and the wavelength-domain is changed from 1600 nm–1700 nm. The best sensitivity is calculated at the temperature of 40 °C for this proposed temperature sensor. The maximum wavelength sensitivity response is recorded 29,411.765 nm/RIU and temperature sensitivity response is recorded 5000 pm/°C at 40 °C. This article shows that the diagonal lengths of air holes have an effect on the recorded wavelength sensitivity and temperature sensitivity response. The sensitivity response is decreased for decreasing diagonal lengths of air holes.

Declaration of Competing Interest

The authors declare that they have no known competing financial interests or personal relationships that could have appeared to influence the work reported in this paper.

Hasan Abdullah
 Md. Rafiqul Islam
 Kawsar Ahmed
 Dror Malka
 Truong Khang Nguyen
 Md. Nadim Hossain
 Bikash Kumar Paul
 Vigneswaran Dhasarathan

References

- [1] J.H. Osório, J.G. Hayashi, Y.A. Espinel, M.A. Franco, M.V. Andrés, C.M. Cordeiro, Photonic-crystal fiber-based pressure sensor for dual environment monitoring, *Appl. Opt.* 53 (17) (2014) 3668–3672.
- [2] Y. Lu, M.T. Wang, C.J. Hao, Z.Q. Zhao, J.Q. Yao, Temperature sensing using photonic crystal fiber filled with silver nanowires and liquid, *IEEE Photonics J.* 6 (3) (2014) 1–7.
- [3] J. Ju, W. Jin, Photonic crystal fiber sensors for strain and temperature measurement, *J. Sens.* 2009 (2009).
- [4] B.K. Paul, E. Rajesh, S. Asaduzzaman, M.S. Islam, K. Ahmed, I.S. Amiri, R. Zakaria, Design and analysis of slotted core photonic crystal fiber for gas sensing application, *Results Phys.* 11 (2018) 643–650.
- [5] P. Hu, X. Dong, W.C. Wong, L.H. Chen, K. Ni, C.C. Chan, Photonic crystal fiber interferometric pH sensor based on polyvinyl alcohol/polyacrylic acid hydrogel coating, *Appl. Opt.* 54 (10) (2015) 2647–2652.
- [6] J. Mathew, Y. Semenova, G. Farrell, Photonic crystal fiber interferometer for dew detection, *J. Light. Technol.* 30 (8) (2011) 1150–1155.
- [7] B.K. Paul, K. Ahmed, D. Vigneswaran, F. Ahmed, S. Roy, D. Abbott, Quasi-photonic crystal fiber-based spectroscopic chemical sensor in the terahertz spectrum: design and analysis, *IEEE Sens. J.* 18 (24) (2018) 9948–9954.
- [8] A. Jana, G. Sharma, A.M. Shrivastav, A.S. Rathore, R. Jha, Photonic crystal fiber based magnetic field sensor realizing Mach-Zehnder interference, *July, Opt. Sens.* (2018) SEW3E-2 Optical Society of America.
- [9] X.Z. Ding, H.Z. Yang, X.G. Qiao, P. Zhang, O. Tian, Q.Z. Rong, N.A.M. Nazal, K.S. Lim, H. Ahmad, Mach-Zehnder interferometric magnetic field sensor based on a photonic crystal fiber and magnetic fluid, *Appl. Opt.* 57 (9) (2018) 2050–2056.
- [10] I.S. Amiri, B.K. Paul, K. Ahmed, A.H. Aly, R. Zakaria, P. Yupapin, D. Vigneswaran, Tri-core photonic crystal fiber based refractive index dual sensor for salinity and temperature detection, *Microw. Opt. Technol. Lett.* 61 (3) (2019) 847–852.
- [11] D. Kumar, D. Kalra, M. Kumar, Analysis of photonic crystal fiber-based micro-strain sensor, *Recent Trends in Communication, Computing, and Electronics*, Springer, Singapore, 2019, pp. 43–50.
- [12] F. Yang, Z.K. Wang, D.N. Wang, A highly sensitive optical fiber strain sensor based on cascaded multimode fiber and photonic crystal fiber, *Opt. Fiber Technol.* 47 (2019) 102–106.
- [13] K. Barczak, Application of photonic crystal fiber in optical fiber current sensors, *Acta Phys. Polonica-Series A Gen. Phys.* 122 (5) (2012) 793.
- [14] H.Y. Fu, H.Y. Tam, L.Y. Shao, X. Dong, P.K.A. Wai, C. Lu, S.K. Khijwania, Pressure sensor realized with polarization-maintaining photonic crystal fiber-based Sagnac interferometer, *Appl. Opt.* 47 (15) (2008) 2835–2839.
- [15] J.H. Osório, J.G. Hayashi, Y.A. Espinel, M.A. Franco, M.V. Andrés, C.M. Cordeiro, Photonic-crystal fiber-based pressure sensor for dual environment monitoring, *Appl. Opt.* 53 (17) (2014) 3668–3672.
- [16] L.E. Horan, F.C.G. Gunning, Hollow core photonic crystal fiber as a viscosity sensor, November, International Society for Optics and Photonics, OFS2012 22nd International Conference on Optical Fiber Sensors, 8421 2012, p. 84216X.
- [17] J. Mathew, Y. Semenova, G. Rajan, G. Farrell, Humidity sensor based on photonic crystal fibre interferometer, *Electron. Lett.* 46 (19) (2010) 1341–1343.
- [18] R.J. Tong, Y. Zhao, M.Q. Chen, Y. Peng, Relative humidity sensor based on small up-tapered photonic crystal fiber Mach-Zehnder interferometer, *Sens. Actuators A Phys.* 280 (2018) 24–30.
- [19] R.K. Verma, B.D. Gupta, Theoretical modelling of a bi-dimensional U-shaped surface plasmon resonance based fibre optic sensor for sensitivity enhancement, *J. Phys. D Appl. Phys.* 41 (9) (2008) 095106.
- [20] M.H. Chiu, S.F. Wang, R.S. Chang, D-type fiber biosensor based on surface-plasmon resonance technology and heterodyne interferometry, *Opt. Lett.* 30 (3) (2005) 233–235.
- [21] H. Gong, X. Yang, K. Ni, C.L. Zhao, X. Dong, An optical fiber curvature sensor based on two peanut-shape structures modal interferometer, *IEEE Photonics Technol. Lett.* 26 (1) (2013) 22–24.
- [22] R.K. Verma, A.K. Sharma, B.D. Gupta, Surface plasmon resonance based tapered fiber optic sensor with different taper profiles, *Opt. Commun.* 281 (6) (2008) 1486–1491.
- [23] S. Pevec, D. Donagic, High resolution, all-fiber, micro-machined sensor for simultaneous measurement of refractive index and temperature, *Opt. Express* 22 (13) (2014) 16241–16253.
- [24] D. Clerc, W. Lukosz, Integrated optical output grating coupler as biochemical sensor, *Sens. Actuators B Chem.* 19 (1–3) (1994) 581–586.
- [25] C. Wu, B.O. Guan, C. Lu, H.Y. Tam, Salinity sensor based on polyimide-coated photonic crystal fiber, *Opt. Express* 19 (21) (2011) 20003–20008.
- [26] P. Dang, K. Le, Q. Ngo, H. Trung Nguyen, T. Nguyen, Guided-mode resonance filter with ultra-narrow bandwidth over the visible frequencies for label-free optical biosensor, *J. Adv. Eng. Comput.* 3 (2019) 406–414.
- [27] K. Le, Q. Ngo, T. Nguyen, Nanostructured metal-insulator-metal metamaterials for refractive index biosensing applications: design, fabrication, and characterization, *IEEE, IEEE J. Selected Topics in Quantum Electron.* 23 (2) (2017) 388–393.
- [28] C. Chen, A. Laronche, G. Bouwmans, L. Bigot, Y. Quiquempois, J. Albert, Sensitivity of photonic crystal fiber modes to temperature, strain and external refractive index, *Opt. Express* 16 (13) (2008) 9645–9653.
- [29] F. Pang, W. Xiang, H. Guo, N. Chen, X. Zeng, Z. Chen, T. Wang, Special optical fiber for temperature sensing based on cladding-mode resonance, *Opt. Express* 16 (17) (2008) 12967–12972.
- [30] Y. Peng, J. Hou, Z. Huang, Q. Lu, Temperature sensor based on surface plasmon resonance within selectively coated photonic crystal fiber, *Appl. Opt.* 51 (26) (2012) 6361–6367.
- [31] D. Wu, Y. Zhao, H. Hu, Experimental research on FLM temperature sensor with an ethanol-filled photonic crystal fiber, *Sens. Actuators A Phys.* 209 (2014) 62–67.
- [32] C.L. Zhao, Z. Wang, S. Zhang, L. Qi, C. Zhong, Z. Zhang, S. Jin, J. Guo, H. Wei, Phenomenon in an alcohol not full-filled temperature sensor based on an optical fiber Sagnac interferometer, *Opt. Lett.* 37 (22) (2012) 4789–4791.
- [33] X. Zheng, Y.G. Liu, Z. Wang, T. Han, C. Wei, J. Chen, Transmission and temperature sensing characteristics of a selectively liquid-filled photonic-bandgap-fiber-based Sagnac interferometer, *Appl. Phys. Lett.* 100 (14) (2012) 141104.

- [34] D. Vigneswaran, N. Ayyanar, M. Sharma, M. Sumathi, M. Rajan, K. Porsezian, Salinity sensor using photonic crystal fiber, *Sens. Actuators A Phys.* 269 (2018) 22–28.
- [35] M.S. Alam, S. Akter, B.K. Paul, K. Ahmed, D. Vigneswaran, M.N. Aktar, FEM based highly sensitive dual core temperature sensor: design and analysis, *OSA Continuum* 2 (9) (2019) 2581–2592.
- [36] Q. Liu, S. Li, H. Chen, Z. Fan, J. Li, Photonic crystal fiber temperature sensor based on coupling between liquid-core mode and defect mode, *IEEE Photonics J.* 7 (2) (2015) 1–9.
- [37] J. Villatoro, V. Finazzi, V.P. Minkovich, V. Pruneri, G. Badenes, Temperature-insensitive photonic crystal fiber interferometer for absolute strain sensing, *Appl. Phys. Lett.* 91 (9) (2007) 091109.
- [38] B. Gauvreau, A. Hassani, M.F. Fehri, A. Kabashin, M. Skorobogatiy, Photonic bandgap fiber-based surface plasmon resonance sensors, *Opt. Express* 15 (18) (2007) 11413–11426.